A Closeness Function on Coarse Grained Lorentzian Geometries

Sumati Surya,

Raman Research Institute, CV Raman Ave, Sadashivanagar, Bangalore 560080, India.

October 23, 2025

Abstract

We construct a family of closeness functions on the space of finite volume Lorentzian geometries using the abundance of discrete intervals in the underlying random causal sets. Although strictly weaker than a Lorentzian Gromov Hausdorff distance function, it has the advantage of being numerically calculable for large causal sets. It thus provides a concrete and quantitative measure of continuumlike behaviour in causal set theory and can be used to define a weak convergence condition for Lorentzian geometries.

1 Introduction

Quantifying the closeness of two spacetimes remains an important open problem in Lorentzian geometry. While an exact isometry is well defined, there is considerable ambiguity in what it means for non-isometric spacetimes to be close, or "approximately isometric". From a physicist's perspective, such a characterisation can help quantify the smallness of a perturbation, which in turn can be used to define a convergence condition.

A quantitative characterisation of closeness is also essential for formulations of quantum gravity in which the continuum spacetime is replaced by a more fundamental, proto-geometric structure, which does not satisfy the regularity requirements associated with the classical theory, as in the causal set approach [1]. Continuum spacetimes thus arise as approximations which are close, but not identical, to the underlying proto-geometry.

The question of closeness of Riemannian spaces is of interest to geometrodynamics and the initial value formulation of general relativity [2, 3, 4]. The superspace S(M) of Riemannian spaces modulo diffeomorphisms corresponds to possible initial spatial geometries. Having a quantitative measure of when two initial spatial geometries are close, therefore helps decide if one can be treated as a perturbation of the other. The distance function in a Riemannian space obeys the triangle inequality and can be used to define the so-called Hausdorff distance between any two of its subspaces. Roughly speaking this distance is obtained by maximising over the minimum distance between a point in one subspace and the points in the other subspace. The Gromov-Hausdorff distance between two spaces is then obtained by minimising this Hausdorff distance over all possible embedding of the two spaces, or equivalently by varying over all possible distances functions over the union of the two spaces [5, 6].

It is not straightforward to apply this construction to Lorentzian spacetimes since the Lorentzian distance function obeys a reverse triangle inequality [7]. Despite this, there has been considerable progress in constructing Lorentzian versions of the Gromov-Hausdorff distance between Lorentzian spacetimes. In [8] Bombelli used the underlying random causal set associated with a causal spacetime to define a closeness function on the space \mathcal{L} of finite volume spacetimes from which he extracted a distance function, subject to an assumption which was recently proved in [9]. Subsequently, Noldus [10, 11] and Bombelli and Noldus [12] used the Lorentzian distance function¹ to define a strong metric on a spacetime, from which a Lorentzian Gromov Hausdorff notion of convergence was constructed on \mathcal{L} . There has been significant progress more recently in rigorously defining convergence conditions, both for Lorentzian geometries, as well as their generalisation to the Lorentzian length spaces of Kunzinger and Sämann [13, 14, 15, 16, 17, 18]. In [19] Sormani and Vega used an extended version of the strong metric constructed from cosmological time functions to define a "null-distance function". This was then used to obtain convergence conditions for globally hyperbolic cosmological spacetimes [20, 21, 22] as well as Lorentzian length spaces [15, 18].

In this work we follow Bombelli's lead and focus on this question from the perspective of causal set theory (CST) which is a discrete approach to quantum gravity [1]. Central to CST is the idea that the causal structure poset (M, \prec) associated with a causal spacetime (M, g) contains all the relevant information about the spacetime, upto a discreteness scale. The approach is inspired by theorems in Lorentzian geometry which state that the causal structure of a distinguishing spacetime determines its conformal class [23, 24, 25].

¹The Lorentzian distance function satisfies the condition: d(p,q) > 0 if p is causally to the past of q and d(p,q) = 0 otherwise.

In CST the spacetime continuum is replaced by a locally finite partially ordered set, a causal set, where the order relation \prec is taken to be irreflexive [1, 26, 27]. Local finiteness encapsulates the assumption of a fundamental spacetime discreteness, which is a cornerstone of CST. This in turn implies that the spacetime continuum must be an emergent entity, arising as an approximation to the underlying proto-geometric structure. In CST this is the random causal set generated by a uniform Poisson point process or sprinkling into the spacetime at a density $\rho = 1/V_c$, where V_c is the d-dimensional discreteness scale. An important aspect of CST is the reconstruction of geometric and topological properties of the continuum spacetime from its underlying random causal set. A fundamental conjecture of CST (its "Hauptvermutung") states that if a causal set is approximated at a given V_c by two different spacetimes, then they must be "approximately isometric", which roughly means that they are identical down to the discreteness scale V_c [9, 28, 29]. Quantifying approximate isometry is however non-trivial, since it requires a notion of closeness on the space of Lorentzian geometries.

The Poisson point process into a finite volume spacetime (M, g) induces a probability distribution $P_n(M, g)$ over the space Ω_n of n-element causal sets. In [8] Bombelli defined a closeness function on the space of finite volume causal Lorentzian spacetimes \mathcal{L} using the $P_n(M, g)$. At finite n this is not a distance function on \mathcal{L} since for every n there exist pairs of non-isometric spacetimes over which the function vanishes. A distance function on \mathcal{L} can however be constructed in the large n limit, subject to an assumption that has recently been proved in [9].

While $P_n(M,g)$ is mathematically well defined, it is highly non-trivial to compute. Ω_n grows as $\sim 2^{n^2/4+o(n^2)}$ [30], making it impossible in real time to find $P_n(M,g)$, even for relatively small values of n and simple spacetimes. Ω_n itself has been explicitly enumerated only upto n=16, which is insufficient to recover any continuum information. Instead of considering the entirety of $P_n(M,g)$, one could use a coarser set of geometric order invariants to define weaker families of closeness functions. A geometric order invariant in a random causal set \mathbf{C} obtained from (M,g), is a labelling invariant quantity in \mathbf{C} (an order invariant) whose expectation value corresponds to a geometric or topological invariant of the spacetime. Many such invariants have been constructed [26, 27] and lend support to the fundamental conjecture of CST. However, a single invariant like a dimension estimator [31, 32] is, in an obvious sense, too coarse grained to be very helpful. One must therefore find a family of order invariants which is numerically calculable, but a better approximation of $P_n(M,g)$.

In this work we consider the family of order-invariants in a causal set obtained by counting

the number, or abundance $N_m(C)$ of m-element order intervals with $m = 0, \ldots n - 1$. An order interval is the discrete analogue of an Alexandrov interval and m is an estimate of its volume in discrete units. Let \mathbf{C}_n denote the random n-element causal set associated with the finite volume region (M, g) of a spacetime. We define the n-interval spectrum of (M, g) as $\mathcal{S}_n(M, g) = \{\langle \mathbf{N}_m^{(n)} \rangle\}$ for $m = 0, \ldots n - 2$, where $\mathbf{N}_m^{(n)}$ denotes the random number associated with the abundance $N_m(C_n)$. While there is no direct geometric or topological analogue for each of the $\mathbf{N}_m^{(n)}$, they form the essential ingredients for the discrete Einstein-Hilbert or Benincasa-Dowker-Glaser action for small values of m [33, 34, 35].

As pointed out in [36], $S_n(M, g)$ contains a surprisingly large amount of information about the spacetime, thus providing a coarse grained but robust characterisation of (M, g), upto the discreteness scale $V_c = \text{vol}(M, g)/n$. This is roughly analogous to the spectrum of a discretised elliptic operator in a Riemannian space. Simulations of $S_n(M, g)$ in different spacetimes suggest that it is a scale-dependent geometric "fingerprint" of (M, g) (see Figs. 3-8). Though it contains strictly less information than $P_n(M, g)$, it defines a new class of L^r closeness functions $\mathcal{D}_n^{(r)}(.,.)$ both over $\Omega_n \times \Omega_n$ as well as over $\mathcal{L} \times \mathcal{L}$. While it satisfies both symmetry and the triangle inequality, $\mathcal{D}_n^{(r)}(.,.)$ vanishes between "interval isospectral" Lorentzian geometries and hence is not a distance function on \mathcal{L} . This spectral degeneracy can in some cases be lifted by including additional order invariants to the spectrum for certain sequences of spacetimes, which gives a (weak) convergence criterion in \mathcal{L} .

In Section 2 we review the results of [36] on the abundance of intervals and the spectrum $S_n(M,g)$ of the random n-element causal set \mathbb{C}_n associated with a finite volume spacetime (M,g). The analytic results of [36] for $S_n(\mathbb{D}^d)$ for a causal diamond \mathbb{D}^d in Minkowski spacetime \mathbb{M}^d provides a concrete example with which to compare simulations. In Section 3 we define a class of L^r closeness functions $\mathcal{D}_n^{(r)}(.,.)$ and an associated notion of convergence. We then use the recent results of Braun [9] to define an approximate isometry between non-isometric spacetimes. Numerical simulations are used throughout to illustrate these ideas and guide our intuition. We end with a summary and discussion in Section 4.

2 Interval Abundances in Causal Sets

Let C_n be an *n*-element causal set, or locally finite partially ordered set, with the order relation between elements denoted by \prec . A labelling of C_n is a bijective map $L: C_n \to \tilde{C}_n$ which is an assignment of a distinct label $L(e) = e_i$, $i \in \{1, ..., n\}$ to each element $e \in C_n$. An order invariant of C_n is a function $f: C_n \to \mathcal{R}$, for some choice of range \mathcal{R} , which is independent of the labelling of C_n . This means that the induced labelled order invariant \tilde{f} , defined by $f = \tilde{f} \circ L$ satisfies $\tilde{f}_1 \circ L_1 = \tilde{f}_2 \circ L_2$ for any pair of labelings $L_{1,2}$ of C_n . An example of an order invariant is the number of related pairs in C_n .

For any $e \prec e'$ in C_n the discrete Alexandrov or order interval is

$$(e, e') = \{e'' | e \prec e'' \prec e\}. \tag{1}$$

(e, e') is called an *m*-element order interval if its cardinality |(e, e')| = m. An order interval is itself not label-invariant since the labelled interval (e_i, e_j) in \tilde{C}_n need not remain invariant. On the other hand, the number or abundance of *m*-element intervals $N_m(C_n)$ in C_n is an order invariant, even in a labelled causal set. For example, $N_0(C_n)$ is the number of links or nearest neighbour relations in C_n and is independent of labelling.

In CST we are not only interested in abstract causal sets, but also those that arise from the continuum approximation defined as follows. A random causal set \mathbf{C} at a discreteness scale $V_c = \rho^{-1}$ is associated with every causal spacetime (M, g), which is generated via a Poisson Point Process (PPP) $\Phi : (M, g) \to_{\rho} \mathbf{C}$, where the ordering of elements is induced by the causal relation \prec_M in (M, g). For a PPP, the probability of finding m-elements in a spacetime region of volume V is given by

$$P_m(V) = \frac{(\rho V)^m}{m!} e^{-\rho V},\tag{2}$$

which implies that $\langle \mathbf{m} \rangle = \rho V$. In CST a causal set is said to be approximated by a spacetime, i.e., is continuumlike, if it is generated from a PPP in this manner. It is important to note that most causal sets cannot be obtained in this way and belong to the Kleitman-Rothschild (KR) class of 3-layer posets which are not continuumlike [30].

An important feature of continuumlike causal sets is that they are non-local in a very specific sense – the set of nearest neighbours or links to an element can span the entire height of a causal set. Thus, the $\mathbf{N}_m^{(n)}$ cannot be estimated from a local counting, as one might do in a fixed valency graph, but is globally determined. For the random causal set \mathbf{C}_n associated with a finite volume spacetime (M, g), the expectation value

$$\langle \mathbf{N}_m^{(n)}(M,g)\rangle = \rho^2 \int_M dV_x \int_{I^+(x)\cap M} dV_y \frac{(\rho \operatorname{vol}(x,y))^m}{m!} e^{-\rho \operatorname{vol}(x,y)}, \tag{3}$$

where $\operatorname{vol}(x,y)$ is the volume of the Alexandrov interval $I^+(x) \cap I^-(y)$ in (M,g). We can therefore associate an *n*-interval-spectrum $\mathcal{S}_n(M,g) \equiv \{\langle \mathbf{N}_m^{(n)}(M,g) \rangle\}$ with the spacetime (M,g), where $m=0,\ldots n-2$. We can similarly define $\mathcal{S}_n(C_n) \equiv \{N_m(C_n)\}$ for any abstract

causal set C_n . In MCMC simulations of causal set dynamics, $\mathcal{S}_n(\mathbf{C})$ has been used as an observable to distinguish between a continuum phase and a non-continuum phase in causal set quantum gravity [37, 38, 39]. Extensive simulations carried out in [36] show that the $\mathcal{S}_n(M,g)$ carries a significant amount of global information about (M,g). Moreover, there is recognisable "continuumlike" features in $\mathcal{S}_n(M,g)$ which differs from $\mathcal{S}_n(C_n)$ for non-continuumlike C_n . Very generally, continuumlike behaviour manifests itself with $N_m(C_n)$ being a monotonically decreasing function of m. By numerically comparing $\mathcal{S}_n(M,g)$ for a variety of spacetimes it is clear that it has more detailed information than this, and carries enough geometric and topological information to distinguish between different continuum spacetimes, even for relatively small n (see Figs. 2- 8) [36].

In general the expression Eqn. (3) is not easy to calculate analytically mainly because

$$\operatorname{vol}(x,y) = \int_{I^{+}(x)\cap I^{-}(y)} \sqrt{-g(z)} d^{d}z \tag{4}$$

itself can be a complicated function with no known closed form expression for a generic spacetime. The simplest calculable case is the d-dimensional Minkowski causal diamond $\mathbb{D}^d \subset \mathbb{M}^d$. In [36] $\langle \mathbf{N}_m^{(n)}(\mathbb{D}^d) \rangle$ was calculated to be

$$\langle \mathbf{N}_{m}^{(n)}(\mathbb{D}^{d}) \rangle = \frac{\Gamma(d)^{2}}{m!} n^{m} \sum_{j=0}^{\infty} \frac{(-n)^{j+2}}{j!(j+m+1)(j+m+2)} \frac{\Gamma(\frac{d}{2}(j+m)+1)\Gamma(\frac{d}{2}(j+m+1)+1)}{\Gamma(\frac{d}{2}(j+m+2))\Gamma(\frac{d}{2}(j+m+3))}, (5)$$

where $n = \rho \text{vol}(M, g)$, and is convergent in the large n limit.

For $m \ll n$, the leading order term for d > 2 was shown to simplify to

$$\langle \mathbf{N}_{m}^{(n)}(\mathbb{D}^{d}) \rangle = n^{2-2/d} \frac{\Gamma(2/d+m)}{m!} \frac{\Gamma(d)}{(d/2-1)(d/2+1)_{d-2}} + o(n^{2-2/d}). \tag{6}$$

On the other hand, it is easy to see that for m comparable to $n \gg 1$, Eqn. (5) goes like e^{-n} , approximately independent of dimension. For $m \ll n$, the leading order dependence on n is m independent, and hence for d > 2 one can define

$$\overline{\mathbf{N}}_{m}^{(n)}(d,n) \equiv \frac{\langle \mathbf{N}_{m}(d,n) \rangle}{\langle \mathbf{N}_{0}(d,n) \rangle} = \frac{\Gamma(2/d+m)}{m!\Gamma(2/d)} + o(n^{-2+2/d}), \tag{7}$$

which is independent of n. For $m \sim n$ on the other hand, the exponential decay dominates and to leading order

$$\overline{\mathbf{N}}_m(d,n) \sim o(1). \tag{8}$$

As discussed in [36] the *n*-interval spectrum can also used to pick out local continuumlike neighbourhoods $\mathcal{N}(e)$ in a causal set as an intrinsic, order theoretic version of a Riemann Normal Neighbourhood (RNN) where the curvature is approximately constant.

2.0.1 Simulations

We now show examples of $S_n(M, g)$ generated via Poisson sprinklings into various spacetime regions. In this work we consider (a) the causal diamond or Alexandrov interval \mathbb{D}^d in Minkowski spacetime for d = 2, ... 8, (b) the thickened causal diamond $\mathbb{D}^d \times \mathbb{I}_t$ in Minkowski spacetime, with d = 2, ... 8 and where $\mathbb{I}_t \equiv (0, t)$ with t = 0.05, 0.1, 0.15, 0.2, 0.25, 0.3 (c) the Minkowski hypercube \mathbb{I}^d for d = 2, ... 8 with two spacelike boundaries (the rest being timelike) and finally (d) FRW spacetime regions with line element

$$ds_d^2 = -dt^2 + a^2(t) \left(\sum_{i=1}^{d-1} dx_i^2 \right)$$
 (9)

for d = 3, ... 9 and scale factors (i) $\mathbf{F}_d(p)$ with $a_p(t) = t^p$, p = 0.33, 0.5, 0.67 and (ii) $\mathbf{dS}_d(c)$ with $a_c(t) = e^{ct}$, and c = 0.025, 0.05, 0.1, 0.15, 0.2. Fig. 1 shows some examples of these regions in d = 3.

Figures 3-8 show examples of $S_n(M, g)$ from these simulations. What is striking about these examples is that each spacetime is associated with a characteristic curve, its "fingerprint". In most of these figures we have used only a single realisation of the sprinkling, to avoid excess computational burden. In order to justify this, in Fig. 2 we show the spectrum for d = 4, n = 10,000 over 30 realisations and also their mean and standard error. While the $\mathbf{N}_m^{(n)}(M,g)$ in a given realisation can vary significantly in absolute terms from the mean, there is a strong self-averaging which means that the deviation from the full spectrum is relatively small. This suggests that even a single realisation is sufficient to determine the spacetime, upto the discreteness scale $\rho^{-1} = \text{vol}(M, g)/n$.

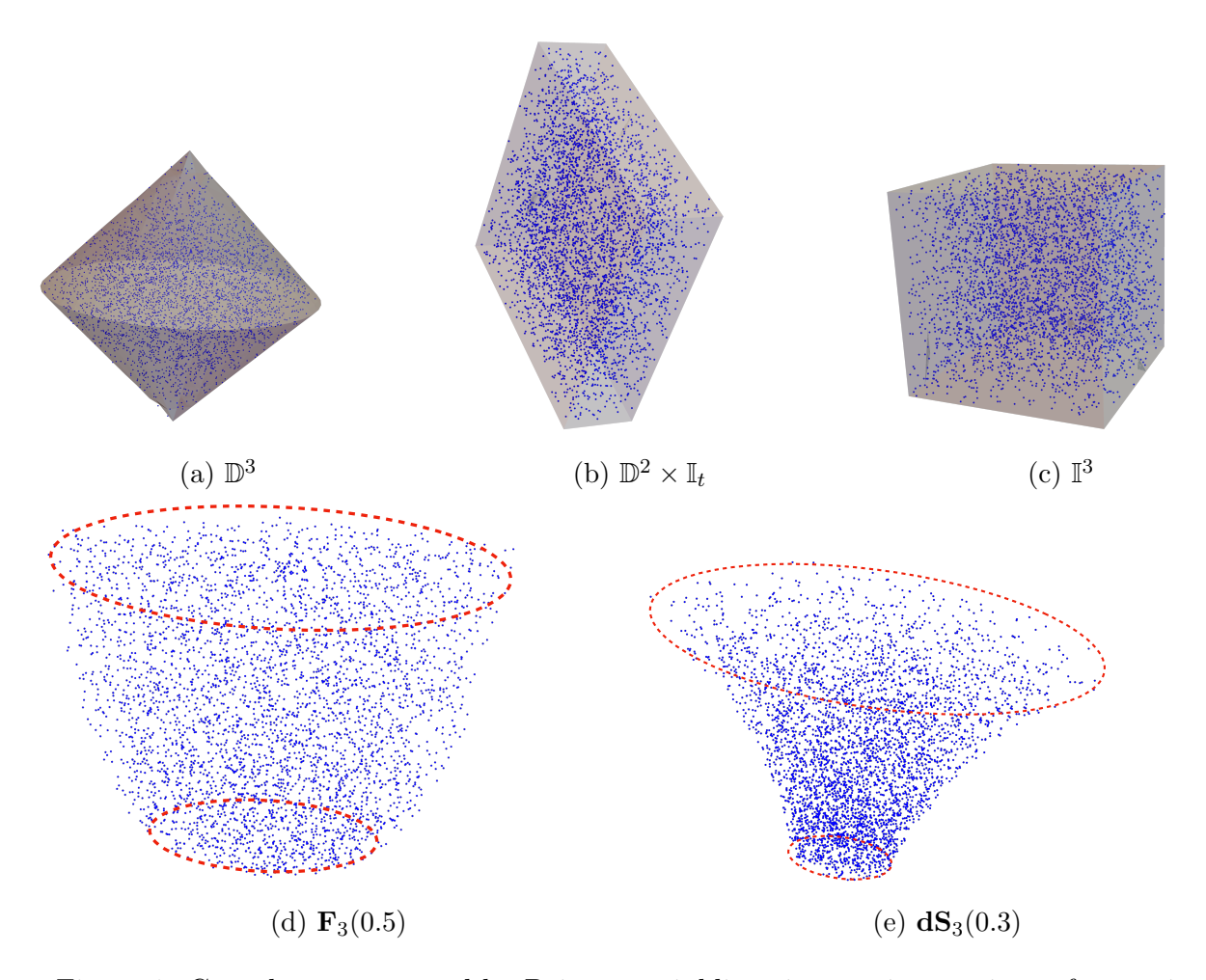


Figure 1: Causal sets generated by Poisson sprinklings into various regions of spacetime.

In Figure 3 the n-interval spectrum $S_n(\mathbb{D}^d)$ is shown for $d=2,\ldots 8$, for n=20,000 elements. The dimension dependence of the curves is explicit and one can therefore use this as an alternative to the flat spacetime Myrheim-Myer dimension estimator [31, 32] as suggested in [36]. In Fig 4 the dimension fixed to d=4 while varying n. There is an obvious scaling with n which also suggests that even at around n=10,000, one is in a fairly reliable large n-regime. In Figure 5 we show the spectrum for a "thickened" diamond $\mathbb{D}^d \times \mathbb{I}_t$, where \mathbb{I}_t represents an "internal" dimension of relative thickness t. The local geometry is Minkowski, but the global features make the spectra distinct. For fixed t, we see a similar behaviour as in the case of the \mathbb{D}^d for d>2, as both d and n are varied. In Fig. 6 we fix d=4, n=20,000 and change the t values. As t is made smaller, it approaches \mathbb{D}^4 , and as it is made larger, it approaches \mathbb{D}^5 , as one would expect. In other words, for a fixed n, there is a small enough t, such that \mathbb{D}^d and $\mathbb{D}^d \times \mathbf{I}$ are n-interval isospectral and cannot be distinguished from each other. In

Figure 7 we consider the hypercube \mathbb{I}^d for d = 3, ..., 8, again in Minkowski spacetime and contrast it with \mathbb{D}^d . The relevance of the global features of the spacetime region are quite explicit. Finally, in Fig. 8 we compare the spectra over a wider range of spacetimes including non-flat, cosmological spacetime regions for fixed n.

It is clear from these Figures and those in [36] that $S_n(M, g)$ differs significantly for spacetimes of different dimensions as well as different geometries. We have not made a comparison here with non-continuum like causal sets and refer the reader to the examples shown in [36]. While the $S_n(M, g)$ bring out qualitative differences and similarities, it is useful to have a quantitative measure of closeness for both extrinsic and intrinsic comparisons in CST.

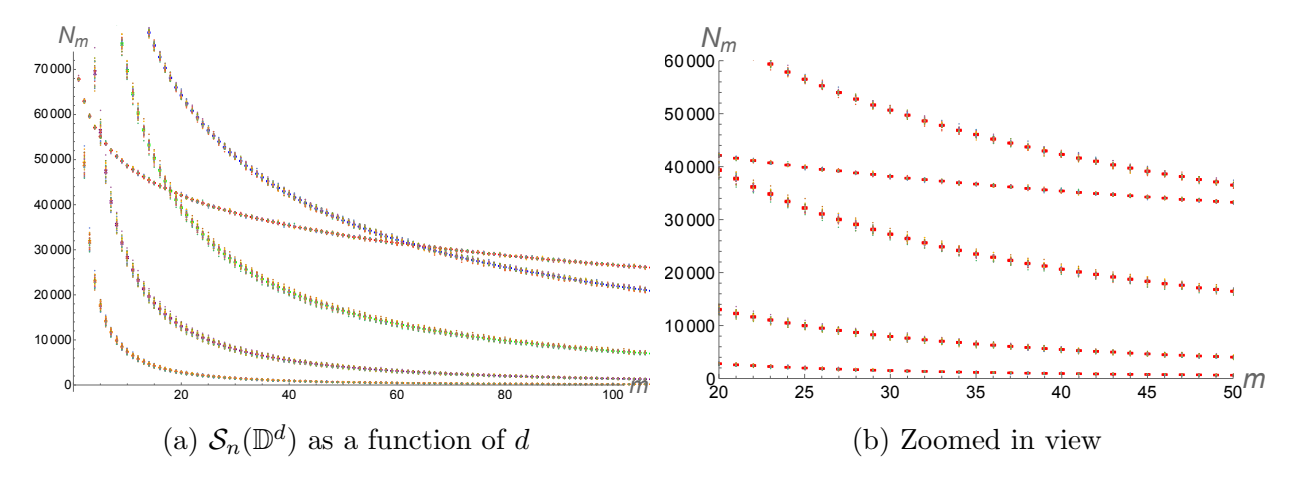


Figure 2: We show 30 different realisations of $S_n(\mathbb{D}^d)$ for n = 10,000, d = 2,...6 plotted with the mean and standard error. One can make out the spread, which is large for any given m, but is relatively small as far as the entire spectrum is concerned. Compare with Fig. 3 below.

3 An *n*-Interval Closeness Function

We begin with the definition of Bombelli's closeness function using $P_n(M,g)$. Let $P_n(C|M,g)$ be the probability that causal set $C \in \Omega_n$ is obtained in a sprinkling into (M,g). Since $1 \geq P_n(C|M,g) \geq 0$ and $\sum_{C \in \Omega_n} P_n(C|M,g) = 1$, P_n maps each spacetime (M,g) onto the non-negative part of the unit sphere, $\mathbb{S}^{|\Omega_n|-1,+} \subset \mathbb{R}^{|\Omega|_n}$, i.e., $P_n : \mathcal{L} \to \mathbb{S}^{|\Omega_n|-1,+}$. Using the angular separation between the points on $\mathbb{S}^{|\Omega_n|-1,+}$ as a measure of closeness in \mathcal{L} , the Bombelli closeness function is

$$\mathcal{D}_B(g_1, g_2) \equiv \frac{2}{\pi} \arccos \sum_{C \in \Omega_n} \sqrt{P_n(C|M_1, g_1)} \sqrt{P_n(C|M_2, g_2)}, \tag{10}$$

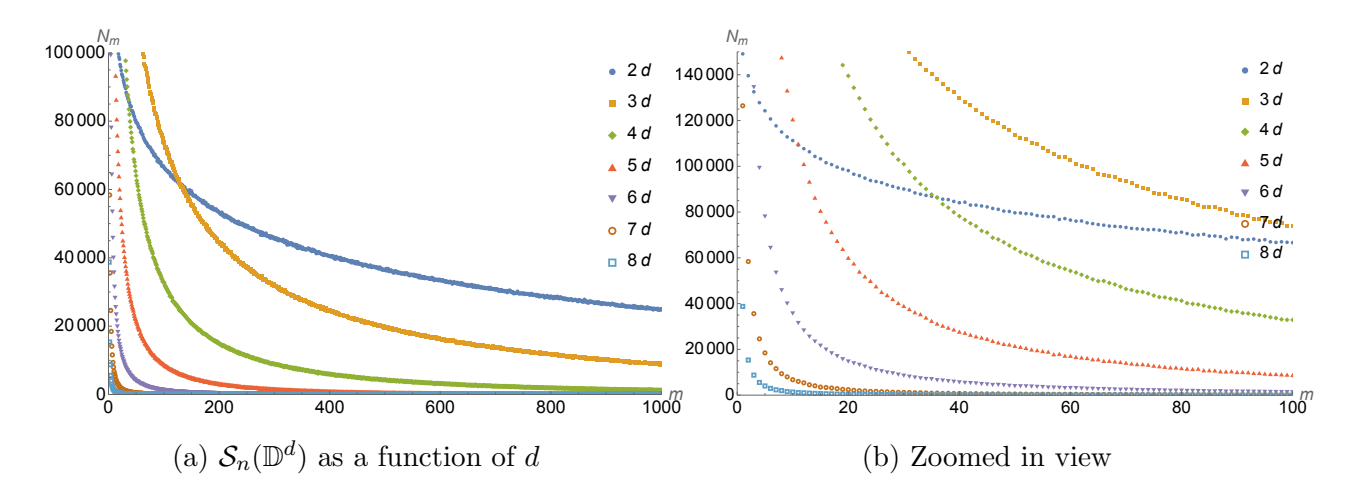


Figure 3: $S_n(\mathbb{D}^d)$ for $d=2,\ldots 8$ for a single realisation with n=20,000.

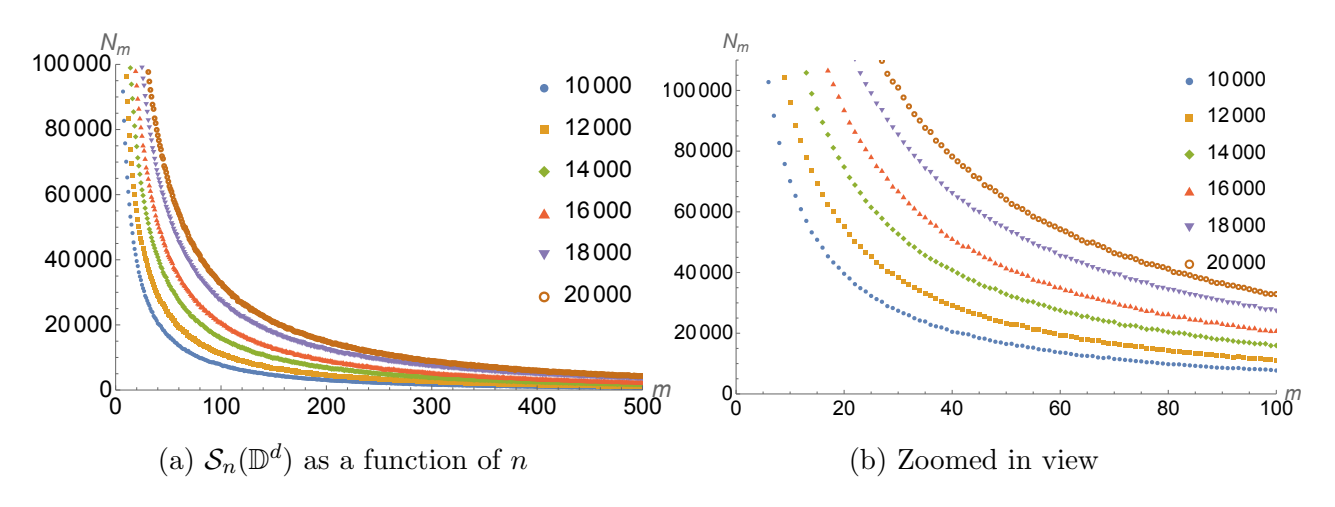


Figure 4: $S_n(\mathbb{D}^4)$ for a range of n values. While the number of intervals increases with the size of the causal set, the overall shape of the function does not change.

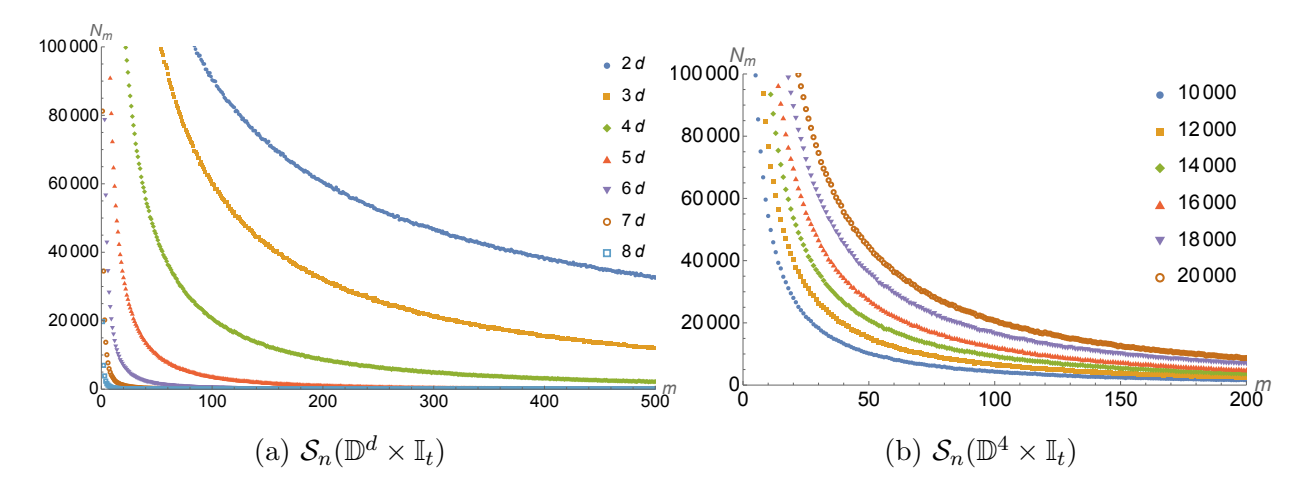


Figure 5: (a) $S_n(\mathbb{D}^d \times \mathbb{I}_t)$ for t = 0.15 and d = 2, ..., 8. (b) $S_n(\mathbb{D}^d \times \mathbb{I}_t)$ for n = 10,000,...20,000. The qualitative behaviour is very similar to that of \mathbb{D}^d .

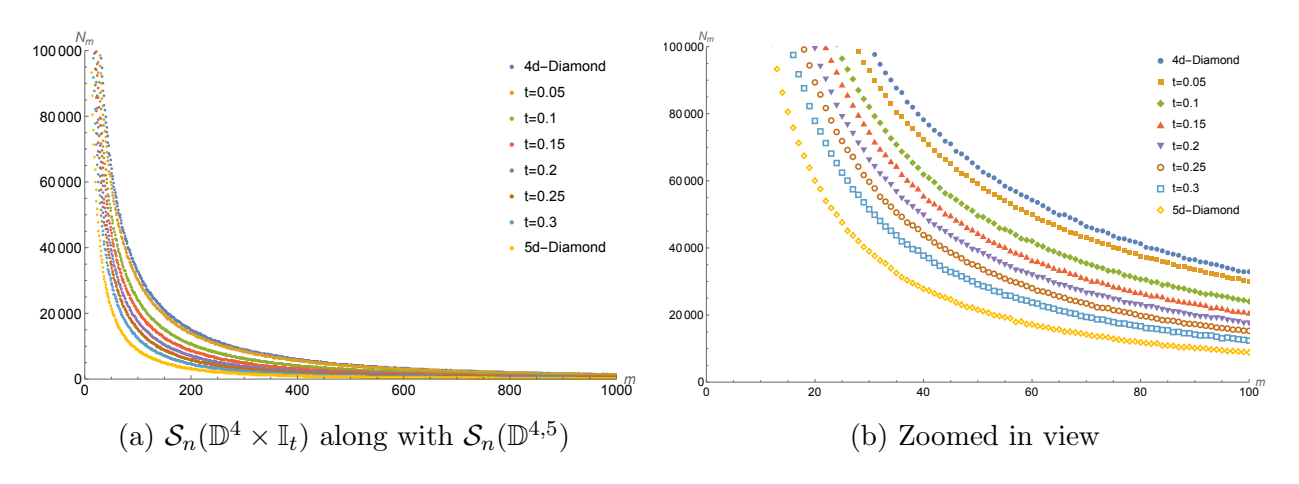


Figure 6: These figures contrast $\mathcal{S}_n(\mathbb{D}^4 \times \mathbb{I}_t)$ with $\mathcal{S}_n(\mathbb{D}^4)$ and $\mathcal{S}_n(\mathbb{D}^5)$, as one changes the relative size t of the internal dimension. One notes the interpolation from $\mathcal{S}_n(\mathbb{D}^4)$ to $\mathcal{S}_n(\mathbb{D}^5)$ as t increases. In particular, there is a convergence to $\mathcal{S}_n(\mathbb{D}^d)$ as t decreases.

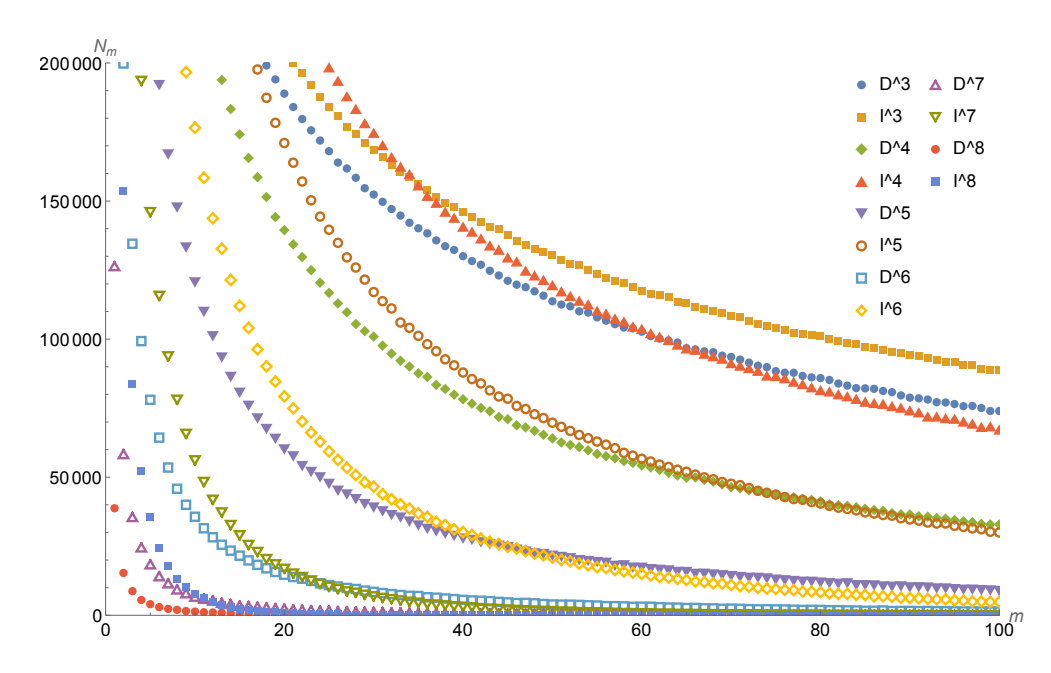


Figure 7: $S_n(\mathbb{I}^d)$ and $S_n(\mathbb{D}^d)$, for d = 3, ... 8, n = 20,000. Even though the spacetime is locally Minkowski, $S_n(.)$ can distinguish the global geometry.

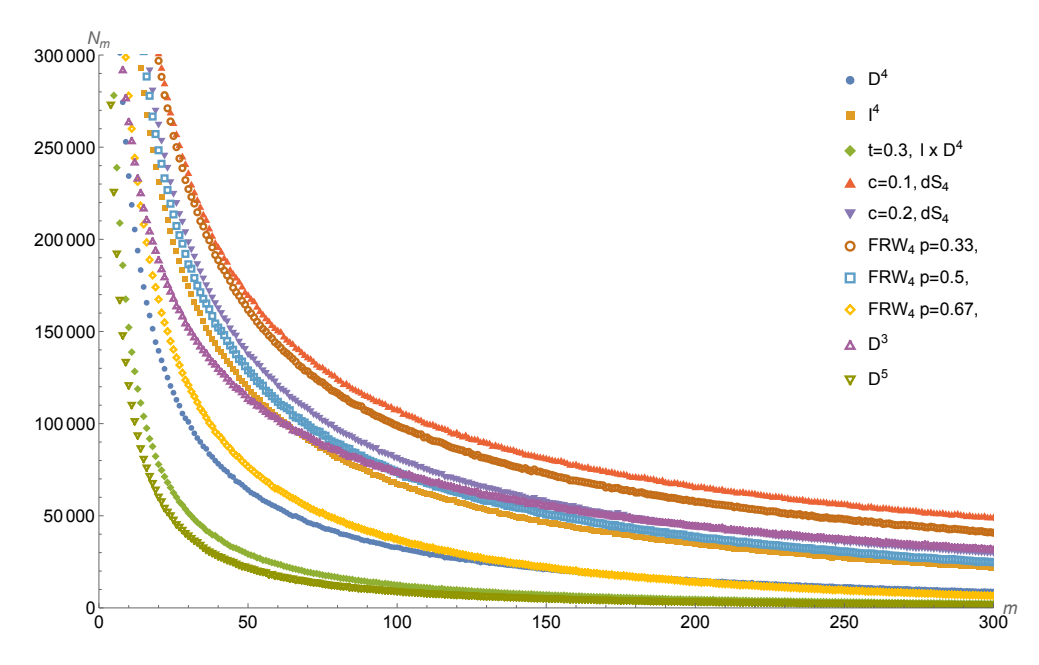


Figure 8: $S_n(.)$ for a range of spacetimes with n = 20,000 shows how well it is able to distinguish between them.

where $(M_i, g_i) \in \mathcal{L}$. For finite n, P_n is not injective: for two spacetimes which are close with respect to V_c , the distribution $P_n(M, g)$ is expected to be the same. Thus, $\mathcal{D}_B(g_1, g_2)$ can vanish between non-isometric spacetimes and is hence not a distance function. However, one expects that as n increases, P_n can resolve the difference between non-isometric spacetimes. Assuming this, one can then construct a distance function on \mathcal{L} [8]. A recent proof by Braun proves this assumption by showing that the (labelled) distributions $P_n(C|M_1, g_1)$ and $P_n(C|M_2, g_2)$ are equal for all n iff g_1 and g_2 are strictly isometric [9].

We will now use the $N_m^{(n)}(C_n)$ and $\mathbf{N}_m^{(n)}(M,g)$ for a similar construction of a closeness function². These are non-negative integers and real numbers, respectively, and having no further restrictions, lie in the non-negative hyperoctant $\overline{\mathbb{R}}^{n-1,+} \subset \mathbb{R}^{n-1}$. In what follows $\overline{\mathbb{Z}}^{n-1,+}$ denotes the n-1 direct product of $\overline{\mathbb{Z}}^+$, the non-negative integers.

We begin by calling two spacetimes n-interval isospectral, if $\forall n' \leq n$, $S_{n'}(M_1, g_1) = S_{n'}(M_2, g_2)$. We denote this equivalence by $(M_1, g_1) \sim_n (M_2, g_2)$, and define the quotient space $\tilde{\mathcal{L}}_n \equiv \mathcal{L}/\sim_n$. A pair of non-isometric spacetimes will be said to be interval isospectral $(M_1, g_1) \sim (M_2, g_2)$ if $S_n(M_1, g_1) = S_n(M_2, g_2) \ \forall n > 0$. This defines the interval isospectral classes [(M, g)] in \mathcal{L} and the associated quotient space $\tilde{\mathcal{L}} \equiv \mathcal{L}/\sim$. For example, distinct pairs of time reversed causal sets or spacetimes are interval isospectral. Other non-trivial discrete transformations on a spacetime can also produce interval isospectral spacetimes, for example the parity operator $x \to -x$ in d = 2. A general classification of interval isospectral spacetimes is of interest – since these have the same discrete Einstein-Hilbert action, they are dynamically equally probable in the quantum gravity path integral.

Define the map $p_n:\Omega_n\to\overline{\mathbb{Z}}^{n-1,+}$ where

$$p_n(C_n) \equiv \{N_0(C_n), N_1(C_n), \dots, N_{n-2}(C_n)\} \in \overline{\mathbb{Z}}^{n-1,+} \subset \overline{\mathbb{R}}^{n-1,+},$$
 (11)

and $N_m(C_n) \in \overline{\mathbb{Z}}^+$. Similarly, let $\pi_n : \mathcal{L}_n \to \overline{\mathbb{R}}^{n-1,+}$, where

$$\pi_n(M,g) \equiv \{ \mathbf{N}_0^{(n)}(M,g), \mathbf{N}_1^{(n)}(M,g), \dots, \mathbf{N}_{n-2}^{(n)}(M,g) \} \in \overline{\mathbb{R}}^{n-1,+}.$$
 (12)

Note that (i) $p_n(\Omega_n)$ and $\pi_n(\mathcal{L})$ are sets of measure zero in $\mathbb{R}^{n-1,+}$, (ii) $p_n(C_n)$ is invariant under relabellings of C_n , and similarly, $\pi_n(M,g)$ is diffeomorphism invariant, and (iii) it is possible for $p_n(C_n) = p_n(C'_n)$, or $\pi_n(M,g) = \pi_n(M',g')$, i.e., p_n and π_n are not injective in general. This means that there cannot be an equivalent of Braun's result for $\pi_n(M,g)$ since non-isometric spaces can be interval isospectral.

²For convenience of notation we henceforth replace $\langle . \rangle$ with the random variable.

We can use any of the possible L^r distance functions on $\overline{\mathbb{R}}^{n-1,+}$ for $r \geq 1$ to define a closeness function between causal sets in Ω_n

$$\mathcal{D}_n^{(r)}(C_n, C_n') = \left(\sum_{m=0}^{n-2} |N_m(C_n) - N_m(C_n')|^r\right)^{1/r},\tag{13}$$

or between spacetimes in \mathcal{L}

$$\mathcal{D}_n^{(r)}(g_1, g_2) = \left(\sum_{m=0}^{n-2} |\mathbf{N}_m^{(n)}(M_1, g_1) - \mathbf{N}_m^{(n)}(M_2, g_2)|^r\right)^{1/r}.$$
 (14)

By definition, $\mathcal{D}_n^{(r)}(.,.)$ satisfies symmetry and the triangle inequality, even though it is possible for $\mathcal{D}_n^{(r)}(.,.) = 0$, i.e., it is not positive. Since our arguments do not depend on the choice of r, we will henceforth choose the simplest, the L^1 "taxi-cab" distance and drop the r label.

We begin with examples from Ω_n . Fig. 9 shows examples of the p_n maps for n=2,3 and 4. Ω_2 consists of the 2-element chain $\mathbf{c}_2=1$ and the 2-element antichain $\mathbf{a}_2=1$. Hence

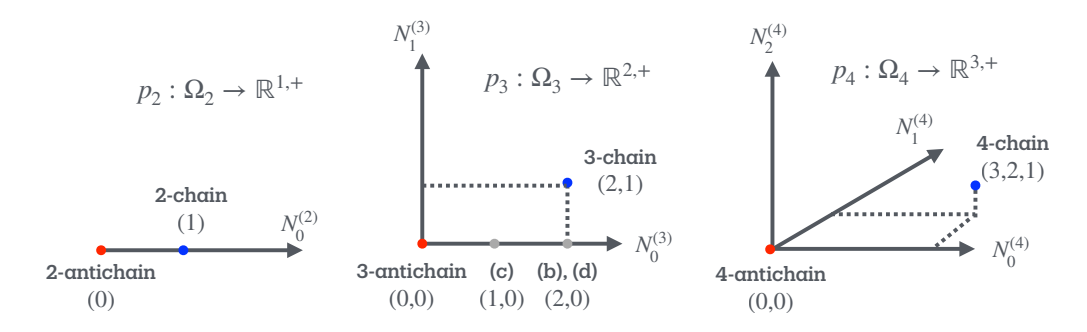


Figure 9: The maps p_2, p_3 and p_4

 $p_2: \Omega_2 \to \mathbb{R}^1$, with $p_2(\mathfrak{z}) = \{1\}$, while $p_2(\cdot \cdot) = \{0\}$. The latter lies at the origin of $\overline{\mathbb{R}}^{1,+}$, and the former at the integer 1. Thus, $\mathcal{D}_2(\mathbf{c}_2, \mathbf{a}_2) = 1$.

The causal sets in Ω_3 are shown in Fig. 10. In order of their appearance in Fig. 10, these causal sets get mapped to the following points in $\overline{\mathbb{R}}^{2,+}$: (2,1), (2,0), (1,0), (2,0) and (0,0) (see Fig. 9). The degeneracy in the spectrum is already evident since the causal sets γ and Λ are time reversals of each other, and hence map to the same point in $\overline{\mathbb{R}}^{2,+}$. The distances between the interval non-isospectral causal sets are $\mathcal{D}_3(\mathbf{c}_3 = \mathbf{1}, \mathbf{a}_3 = \cdots) = 3$, $\mathcal{D}_3(\mathbf{1}, [\gamma]) = 1$, $\mathcal{D}_3(\mathbf{1}, \mathbf{1}, \cdots) = 2$, $\mathcal{D}_3([\gamma], \mathbf{1}, \cdots) = 1$, where $[\gamma]$ refers to either γ or Λ .

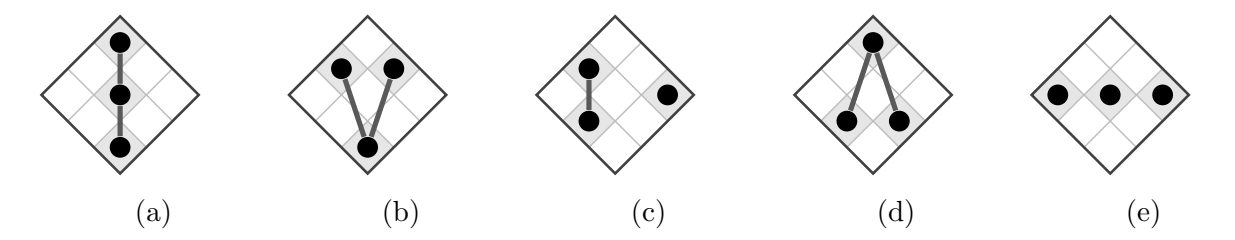


Figure 10: The set Ω_3 of n=3-element unlabelled posets.)

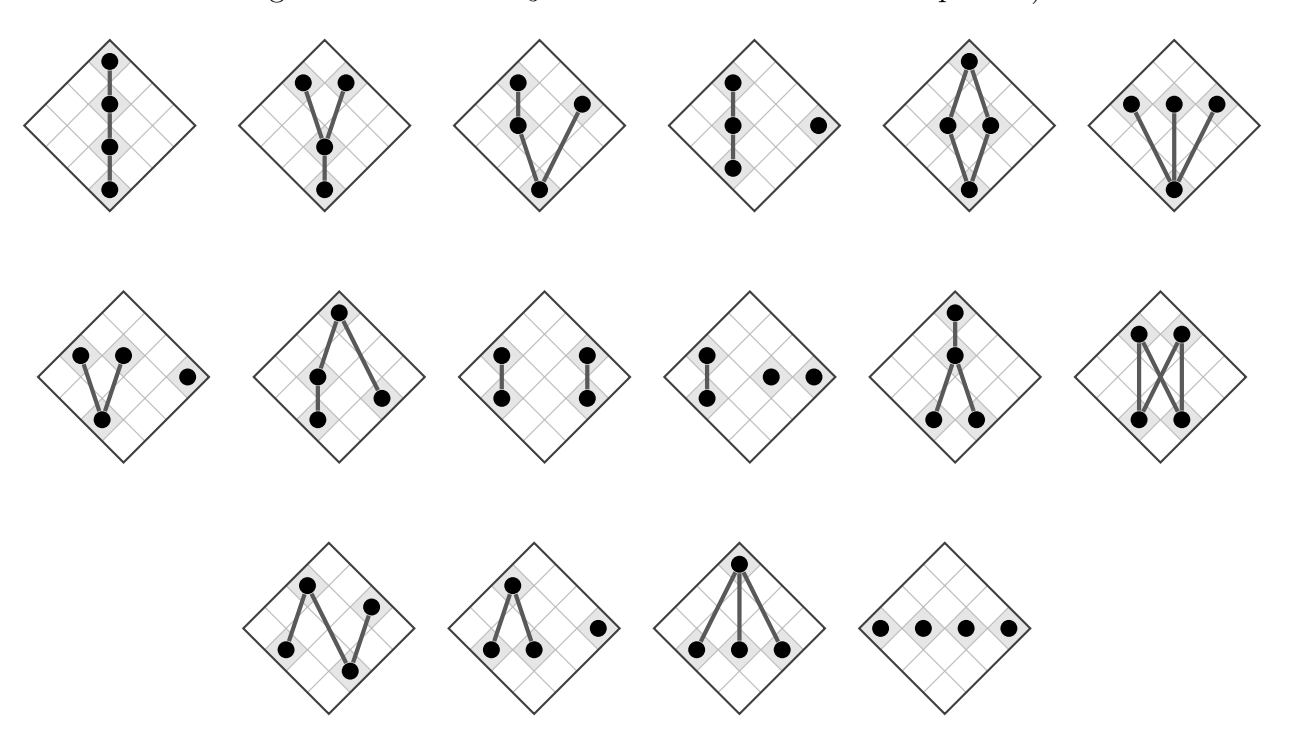


Figure 11: The set Ω_4 of n=4-element unlabelled posets

The non-trivial degeneracies become evident as one moves to Ω_4 as depicted in Fig 11. $p_n(\Omega_4)$ is given by the list (from left to right):

$$\{\{3,2,1\},\{3,2,0\},\{3,1,0\},\{2,1,0\},\{4,0,1\},\{3,0,0\},\{2,0,0\},\{3,1,0\},\{2,0,0\},\\ \{1,0,0\},\{3,2,0\},\{4,0,0\},\{3,0,0\},\{2,0,0\},\{3,0,0\},\{0,0,0\}\}.$$
 (15)

Apart from pairs of time-reversed causal sets, one finds two other non-trivial degeneracies in the spectra: (i) ψ and ψ and (ii) : : and ψ .

One way to break the degeneracy in the spectrum is to include new coordinates. For example, to distinguish between some of the time-reflected causal sets, one could include the sizes of the initial and the final antichains. For Ω_3 this is enough to lift the degeneracy. For Ω_4 , this

lifts the first non-trivial degeneracy but not necessarily the second, if all unrelated elements are considered to be in the initial antichain. In this specific instance, we can distinguish the causal sets by also counting the number F_m of elements with m elements in their future, and similarly the number P_m of elements with m elements in their past.

It becomes rapidly more difficult to repeat this calculation for larger n, since $|\Omega_n| \sim 2^{\frac{n^2}{4} + o(n^2)}$ for large n. However the simplicity of the n-element chain \mathbf{a}_n and \mathbf{c}_n allows us an easy analytic calculation. For these causal sets, the coordinates in $\overline{\mathbb{R}}^{n-1,+}$ are

$$p_n(\mathbf{a}_n) = (0, 0, \dots, 0), \ p_n(\mathbf{c}_n) = (n - 1, n - 2, n - 3, \dots, 1),$$
 (16)

and hence

$$\mathcal{D}_n(\mathbf{a}_n, \mathbf{c}_n) = \frac{(n-1)(n)}{2} \sim n^2/2, \tag{17}$$

for large n. We can also calculate p_n for slightly more complicated causal sets, like the n-element "L" poset \mathbf{L}_n obtained by inserting a single link between two elements of \mathbf{a}_n as well as the n-element "Y" poset \mathbf{Y}_n obtained by removing the maximal element of \mathbf{c}_n and linking it to the $(n-2)^{\text{th}}$ (or last but one) future most element of $\mathbf{c}_{n-1} \subset \mathbf{c}_n$. For these

$$p_n(\mathbf{L}_n) = (1, 0, \dots, 0), \ p_n(\mathbf{Y}_n) = (n - 1, n - 2, n - 3, \dots, 2, 0),$$
 (18)

and

$$\mathcal{D}_{n}(\mathbf{a}, \mathbf{L}_{n}) = \mathcal{D}_{n}(\mathbf{c}, \mathbf{Y}_{n}) = 1, \qquad \mathcal{D}_{n}(\mathbf{a}, \mathbf{Y}_{n}) = \frac{(n-1)(n)}{2},$$

$$\mathcal{D}_{n}(\mathbf{c}, \mathbf{L}_{n}) = \frac{(n-1)(n)}{2} - 1 \qquad \mathcal{D}_{n}(\mathbf{L}_{n}, \mathbf{Y}_{n}) = \frac{(n-1)(n)}{2} - 2. \tag{19}$$

Thus, as n increases, the closeness function between \mathbf{a}_n and \mathbf{c}_n increases, as does that between \mathbf{a}_n and \mathbf{Y}_n , \mathbf{c}_n and \mathbf{L}_n and \mathbf{L}_n and \mathbf{Y}_n . All these functions grow as $n^2/2$. However, the closeness function between \mathbf{a}_n and \mathbf{L}_n , as well as that between \mathbf{c}_n and \mathbf{Y}_n is independent of n and hence relatively speaking, they get closer to each other as n increases, while remaining spectrally distinct from each other for all n. This ties in with our intuition that for large n, the differences between \mathbf{a}_n and \mathbf{L}_n wash out, as do those between \mathbf{c}_n and \mathbf{Y}_n .

While expanding the repertoire of causal sets for which $\mathcal{D}_n(.,.)$ is analytically calculable is an interesting exercise in combinatorics, our main goal here is to use it on \mathcal{L} , the space of all finite volume spacetimes. By fixing n but not the spacetime volumes, we can use $\mathcal{D}_n(.,.)$ to compare spacetimes of different volumes. For example, consider the product spacetime $(M,g) = (M_1 \times M_2, g_1 \otimes g_2)$, where M_2 is an "internal" compact space, with $\rho^{-1} = \text{vol}(M)/n \gg \text{vol}(M_2)$. In this case we expect $\mathbf{C}_n(M,g)$ and $\mathbf{C}_n(M_1,g_1)$ to be very

similar, since the sprinkling is too coarse to see the internal manifold (M_2, g_2) and thus only captures aspects of (M_1, g_1) . As n increases, however, the differences in $\mathbf{C}_n(M, g)$ and $\mathbf{C}_n(M_1, g_1)$ will begin to manifest themselves. While $\mathcal{D}_n(g, g_1) \approx 0$ for $n \ll \text{vol}(M)/\text{vol}(M_2)$, we would expect it to increases with n, thus pushing the spacetimes further apart. In our simulations we have illustrated this in the spectral comparisons of \mathbb{D}^d with its "thickened" version $\mathbb{D}^d \times \mathbb{I}_t$, in Figs. 5 and 6 and the closeness function in Fig. 19.

We would like to use $\mathcal{D}_n(.,.)$ as a measure of an approximate, n-isometry between spacetimes, but because of interval isospectrality, we will need to be careful. If two spacetimes are n-interval isospectral and further, there exists an $n_0 > n$ such that $\forall n' > n_0$ $(M_1, g_1) \nsim_{n'} (M_2, g_2)$, then from Braun's result [9] we know that $P_{n'}(M_1, g_1) \neq P_{n'}(M_2, g_2)$ and hence (M_1, g_1) and (M_2, g_2) are strictly non-isometric. Hence, in a well defined sense, (M_1, g_1) and (M_2, g_2) can be said to be approximately n-interval isometric in \mathcal{L} . Thus, even if we cannot hope to extend this definition to all non-isometric pairs of spacetimes, we can still give a precise notion of approximate isometry for a sub-class of spacetimes. We define the following convergence condition on $\tilde{\mathcal{L}}$:

Definition. Consider a sequence of equivalence classes of finite volume spacetimes $\{[(M_i, g_i)]\}$, $[(M_i, g_i)] \in \tilde{\mathcal{L}}$. We will say that it interval-converges to $[(M, g)] \in \tilde{\mathcal{L}}$ if for every $\epsilon > 0$ and n > 0, there exists an $i_0 > 0$ such that for all $i > i_0$, $\mathcal{D}_n([(M_i, g_i)], [(M, g)]) < \epsilon$. We will say that $\{[(M_i, g_i)]\}$ are (ϵ, n) -close to [(M, g)] for $i > i_0$.

As n increases, the closeness function between non-interval isospectral spacetimes should typically increase. Hence if $\{[(M_i, g_i)]\}$ is (ϵ, n) - close to [(M, g)], then it need not be (ϵ, n') -close to [(M, g)] for n' > n. One can also tie n to ϵ by defining $\epsilon = 1/F(n)$, where F(n) is a monotonically increasing function of n, to define a stricter 1/F(n)-closeness, with $\mathcal{D}_n([(M_i, g_i)], [(M, g)]) < 1/f(n)$.

Despite being strictly defined only on $\hat{\mathcal{L}}$, this convergence criterion can be usefully applied to special classes of spacetimes in \mathcal{L} . Consider for example a one parameter family $\{g(s)\}$ of cosmological FRW spacetimes where the scale factor is given by $a_s(t) = t^{f(s)}$ or, in the case of de Sitter, $a_s(t) = e^{f(s)t}$. Let f(s) > 0 be a monotonically increasing function of s. Consider a sequence of spacetimes $\{a_{s_i}(t)\}$, or equivalently a sequence of functions $\{f(s_i)\}$ such that $\lim_{s_i \to \infty} f(s_i) = f_0 < \infty$, equivalently, $\lim_{s_i \to \infty} a_{s_i}(t) = a_0(t)$.

This sequence of (non-isometric) montonically expanding FRW and de Sitter are also not interval isospectral as we now argue.

Consider two spacetimes $(M, g(s_1))$ and $(M, g(s_2))$, with $s_1 < s_2$. Let us assume that ρ is

a constant, and compare the interval spectrum of equal volume regions of the spacetimes, i.e., $\operatorname{vol}(M, g(s_1)) = \operatorname{vol}(M, g(s_2))$. Since the $g(s_i)$ are conformally related, the continuum Alexandrov intervals $(p, q)_{s_i}$ remain the same, but their volumes do not, i.e., $\operatorname{vol}((p, q)_{s_1}) < \operatorname{vol}((p, q)_{s_2})$. Hence on average, every m_1 -element interval in $(M, g(s_1))$ is an m_2 -element interval in $(M, g(s_2))$ where $m_2 > m_1$, i.e., $\mathbf{N}_{m_2}(s_2) = \mathbf{N}_{m_1}(s_1)$. Since \mathbf{N}_m is a monotonically decreasing function of m, $\mathbf{N}_{m_1}(s_2) > \mathbf{N}_{m_2}(s_2) = \mathbf{N}_{m_1}(s_1)$. Thus, these spacetimes are not interval isospectral. It is important to note that there are no smoothness assumptions on $a_{c,p}(t)$ as a function of c, p or even t.

How does this square with our simulations? An example of this expected behaviour is shown in Fig. 12a for small values of m. However, because we fix n, and consider different volumes of the spacetime regions, the analytic argument is too simplistic (or equivalently our simulations are too limited) to explain the behaviour for all m. In particular, in our simulations of dS_d and F_d we have fixed the initial and final coordinate times, for different scale factors. While the small m behaviour is as we expect analytically, there is a cross over at larger m values with $N_m(s_1) > N_n(s_2)$ for $s_1 < s_2$. This is because the small m values are less affected by boundary effects, while for large m, they do matter. In particular, the spacetime region grows "wider" with increasing s_i , and thus there are fewer large m intervals. In either case, the simulations support the overall argument that these spacetimes are not interval isospectral. Figures 12b and 12c show simulations comparing the interval spectra for $dS_5(c)$, $a_c(t) = e^{ct}$ for different values of c. For n = 10,000 the spectra for c = 0.025, 0.05 and 0.1 lie almost on top of each other, but for n = 20,000, the c = 0.1spectrum is distinguishable from the others. In Fig. 12d the interval spectrum $a_n(t) = t^p$ is shown for p = 0.33, 0.5, 0.67. In principle we could include both monotonically increasing and decreasing functions of t to our set of FRW-type spacetimes, i.e., expanding and contracting spacetimes, and lift the degeneracy in the n-interval spectrum by including the sizes of the initial and final antichains as an additional pair of order invariants, with the closeness function now calculated in $\mathbb{R}^{n+1,+}$. The interval-convergence condition would then trivially extended to this larger space, with contracting and expanding spacetimes being strictly not (ϵ, n) close to each other for arbitrarily large n.

Since we have an analytic expression Eqn. (5) for the $\mathbf{N}_m^{(n)}(\mathbb{D}^d)$, we can begin by testing the closeness function by varying the dimension. For small n, $\mathcal{D}_n(\mathbb{D}^{d_1}, \mathbb{D}^{d_2})$ varies exactly as one might wish, growing as the difference in dimension grows. However, for large n, from Eqn. (6) we see that $\mathcal{D}_n(\mathbb{D}^{d_1}, \mathbb{D}^{d_2})$ grows like $n^{2-2/d}$, where $d = maximum(d_1, d_2)$. Hence, the contribution to the closeness function is dominated by $|\mathbf{N}_m^{(n)}(\mathbb{D}^d)|$. This in turn means that as n becomes larger, \mathbb{D}^d becomes equally far away from all $\mathbb{D}^{d'}$ for d' < d.

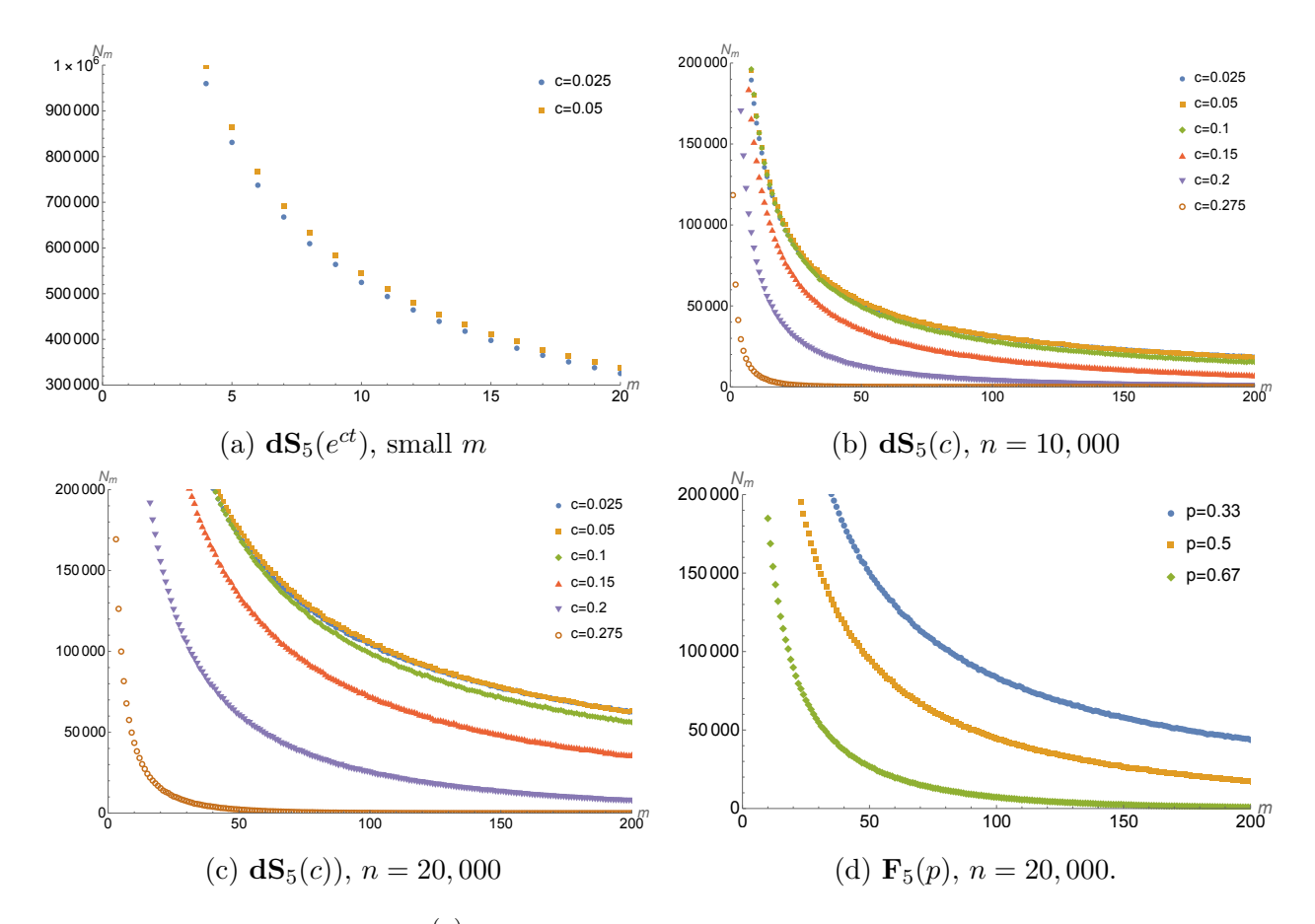


Figure 12: Fig. (a) shows $\mathbf{N}_m^{(n)}$ for smaller values of m for $\mathbf{dS}_5(e^{ct})$ with two different scale factors c=0.025,0.05 for n=20,000. Figs. (b) and (c) show $\mathbf{dS}_5(e^{ct})$ for larger m values for a range of c values for n=10,000 and 20,000. One can see how the n-interval spectral degeneracy is lifted as n increases. Fig. (d) shows the n-interval spectra for FRW spacetimes $\mathbf{F}_5(t^p)$ for p=0.33,0.5,0.67.

It is possible to replace the $\mathbf{N}_m^{(n)}(M,g)$ by the normalised $\overline{\mathbf{N}}_m^{(n)}(M,g)$ in Eqn. (7), which is independent of n to leading order. The "normalised" closeness function is then

$$\bar{\mathcal{D}}_n((M_1, g_1), (M_2, g_2)) = \sum_{m=0}^{n-2} |\overline{\mathbf{N}}_m^{(n)}(M_1, g_1) - \overline{\mathbf{N}}_m^{(n)}(M_2, g_2)|.$$
 (20)

While this can lead to better convergence conditions for large n, it doesn't satisfy the triangle inequality which makes it less desirable to work with.

3.0.1 Simulations

We show examples of $\mathcal{D}_n(.,.)$ using the *n*-interval spectra $\mathcal{S}_n(.)$ of the various types of spacetime regions shown in Fig.1. These simulations show that the closeness function behaves in a manner one expects in simple cases, but also uncovers new features. For example, it is not always the case that the closeness function between spacetimes of different dimensions increases with the difference in dimension – other geometric features can make them closer to lower or higher dimensional spacetimes with different geometries.

Figure 13 shows the closeness function $\mathcal{D}_n(\mathbb{D}^{d_1}, \mathbb{D}^{d_2})$ as one varies over d_1, d_2 for $d_i = 2, ... 8$ for n = 10,000, and over 30 trials. The closeness function increases monotonically with $|\Delta d|$ where $\Delta d \equiv (d_1 - d_2)$, but the rate of change depends on Δd . For fixed d_1 , and $d_2 < d_1$ the rate of change increases with $|\Delta d|$ while for $d_2 > d_1$, it decreases with $|\Delta d|$. Because there is no significant difference between trials, as before we use a single realisation of the sprinkled causal set.

Figure 14 shows how the distance $\mathcal{D}_n(\mathbb{D}^4, \mathbb{D}^d)$ changes as a function of n as one varies d. Figure 15a shows the closeness function $\mathcal{D}_n(\mathbb{D}^4 \times \mathbb{I}_t, \mathbb{D}^d \times \mathbb{I}_t)$ for thickness t = 0.05 for both spacetimes. The behaviour in this case is similar to that of the \mathbb{D}^d shown in Fig. 14. Fig. 15b compares $\mathcal{D}_n(\mathbb{D}^4 \times \mathbb{I}_t, \mathbb{D}^d \times \mathbb{I}_t)$ between t = 0.05 and different thicknesses. As t increases, there is an interesting cross over where the closeness function between d = 4, t = 0.05 and d = 2, 3 decreases as t increases. One can see that this is reasonable: as the thickness of $\mathbb{D}^3 \times \mathbb{I}_t$ increases, it becomes closer to $\mathbb{D}^4 \times \mathbb{I}_{0.05}$.

Next, in Fig. 16 we illustrate the behaviour of $\mathcal{D}_n(.,.)$ between spacetimes of the same kind, but with varying dimensions. Again, the qualitative behaviour is very similar to Fig. 14. We see that $\mathcal{D}_n(.,.)$ between spacetimes of the same kind, but of different dimensions grows with $|\Delta d|$, but that the rate of change of depends on the sign of Δd .

In Fig. 17 we compare different FRW $\mathbf{F}_d(t^p)$ spacetimes for different d and p values. In these plots we see that the geometry can play a more dominant role than the topological

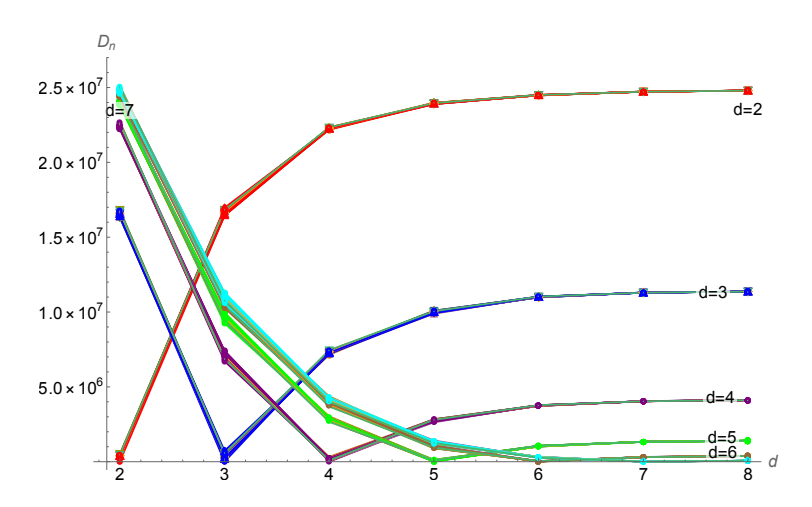


Figure 13: The figure shows $\mathcal{D}_n(\mathbb{D}^d, \mathbb{D}^{d'})$ for n = 10,000 and $d = 2, \dots, 7$ and $d' = 2, \dots, 8$, over 30 trials.

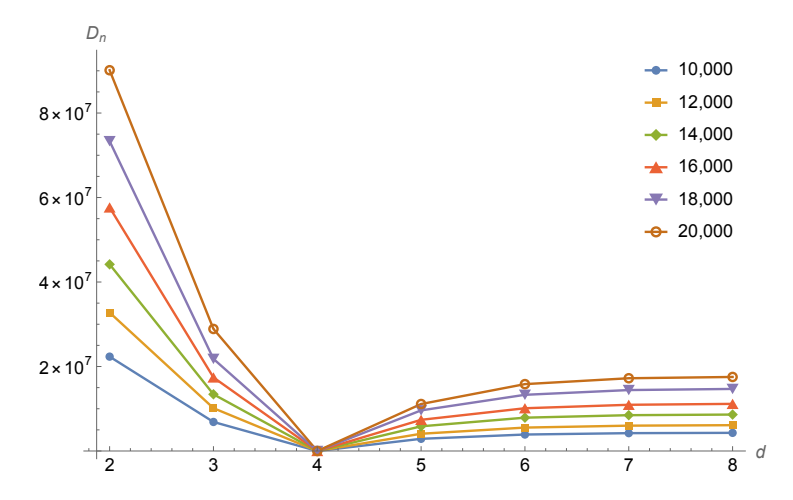


Figure 14: The figure shows $\mathcal{D}_n(\mathbb{D}^4, \mathbb{D}^d)$ for a range of n values as $d = 2, \dots, 8$.

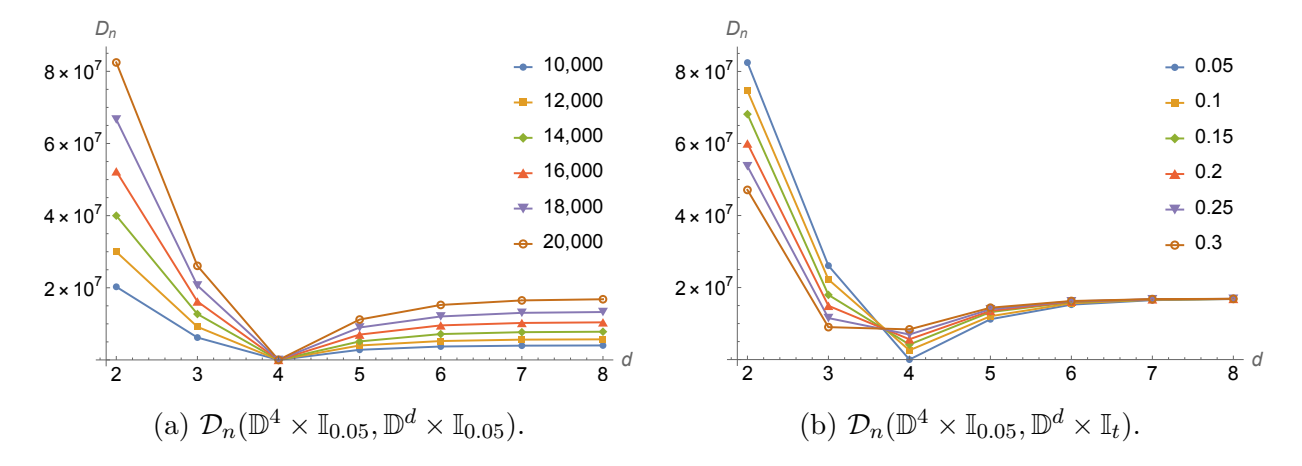


Figure 15: $\mathcal{D}_n(\mathbb{D}^4 \times \mathbb{I}_{0.05}, \mathbb{D}^d \times \mathbb{I}_t)$ as a function of dimension d = 2, ..., 8. (a) t = 0.05 is fixed and n is varied. (b) n = 20,000 and t is varied.

dimension. In all these cases, and for $p_1 \neq p_2$, $\mathcal{D}_n(\mathbf{F}_4(t^{p_1}), \mathbf{F}_d(t^{p_2}))$ is smaller for d = 3 than for d = 4.

In Fig. 18 we compare the different de Sitter spacetimes $\mathbf{dS}_d(e^{ct})$. Here, the interplay between geometry and topological dimension is more evident. Between smaller c values, topological dimension remains more important than the geometry, but as the difference in c values increases, this reverses.

In Fig. 19 we find $\mathcal{D}_n(.,.)$ between \mathbb{D}^4 and $\mathbb{D}^d \times \mathbb{I}_t$ as t varies. Here for smaller t values, the geometry is more important, for example with $\mathbb{D}^4 \times \mathbb{I}_{0.05}$ being closer to \mathbb{D}^4 than to $\mathbb{D}^3 \times \mathbb{I}_{0.05}$, as one might expect. There is a cross over as t increases. For t = 0.3 \mathbb{D}^4 gets closer to $\mathbb{D}^3 \times \mathbb{I}_{0.3}$ than $\mathbb{D}^3 \times \mathbb{I}_{0.3}$ which again not surprising.

Finally, in Fig. 20 we show $\mathcal{D}_n(\mathbb{D}^d, .)$ for different spacetimes. Again we see cases where the topological dimension dominates the geometry and vice-versa.

An important feature of $\mathcal{D}_n(.,.)$ is that it is strictly global in character. Hence even if the spacetime regions are locally isometric, their global "shapes" determine closeness. For example, the causal diamond and hypercube, both in Minkowski spacetime, differ in their n-interval-spectrum and are hence are not arbitrarily close. This global character is also a feature of Bombelli's distance function [8]. A local comparison can be made by extracting a causal diamond from the hypercube and comparing with an equal volume causal diamond.

These figures are illustrative – we have not shown our extensive data, but they corroborate the general features shown here. The simulations of $S_n(.)$ themselves were intensive, with

some parameter values taking several days to compute on a high performance cluster. Since we are not (at least at this stage) interested in the actual value of $\mathcal{D}_n(.,.)$ but only its qualitative features, one might want to simplify simulations in the future by considering only a subset of the m's, for example all $m \leq n/2$. For the range of n values we have considered, perhaps one could even stop at m = 100. However, this makes the definition somewhat ad-hoc, and while this might be justified a posteriori in specific cases, it is more natural to use all the n-1 values of m.

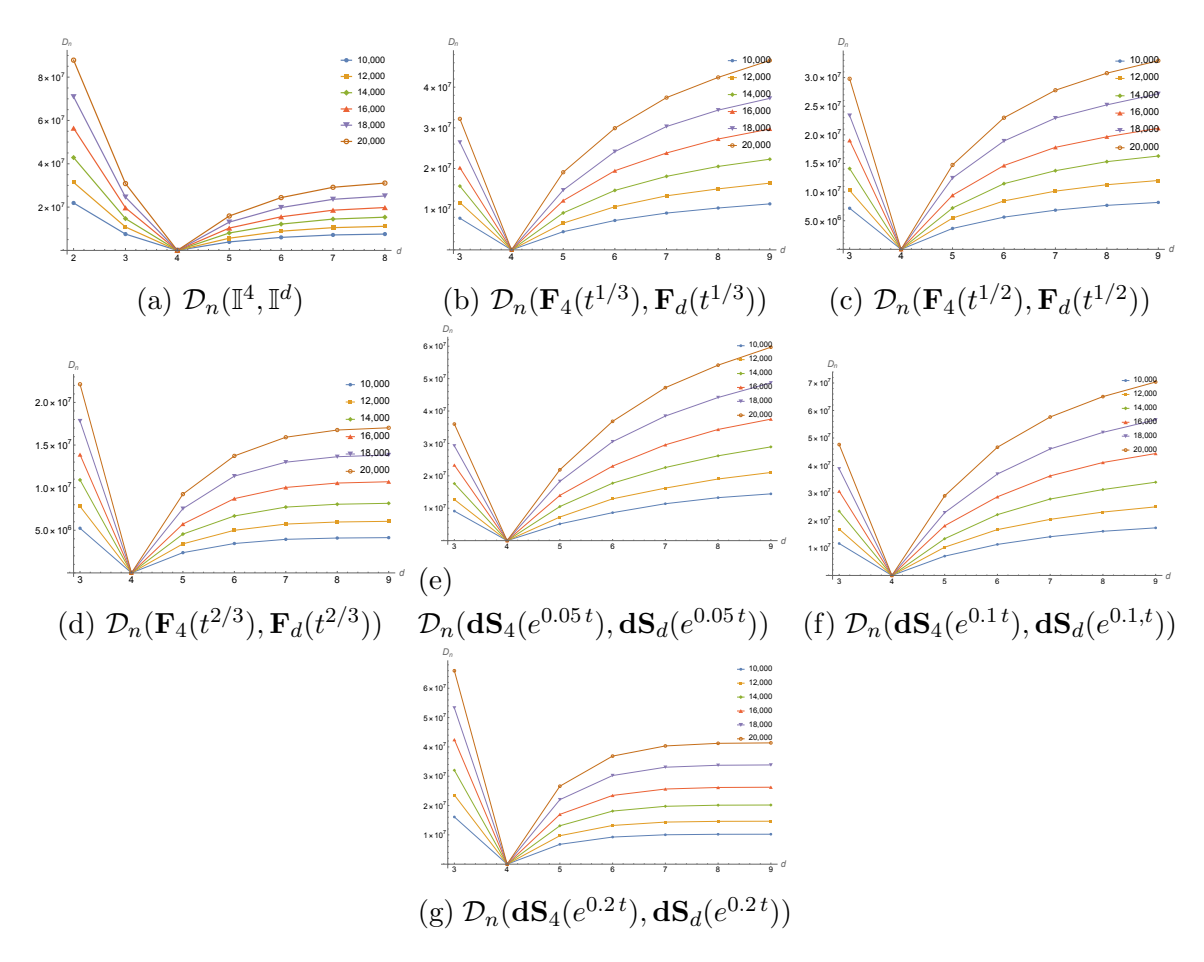


Figure 16: The $\mathcal{D}_n(4,d)$ between a spacetimes of dimension 4 and d, within the same geometric class of spacetimes. The behaviour is similar to that of $\mathcal{D}_n(\mathbb{D}^4,\mathbb{D}^d)$ in Fig. 14.

4 Summary and Discussion

In this work we have proposed a new closeness function $\mathcal{D}_n^{(r)}(.,.)$ on the space of finite volume causal Lorentzian geometries \mathcal{L} . $\mathcal{D}_n^{(r)}(.,.)$ satisfies the triangle inequality, but is

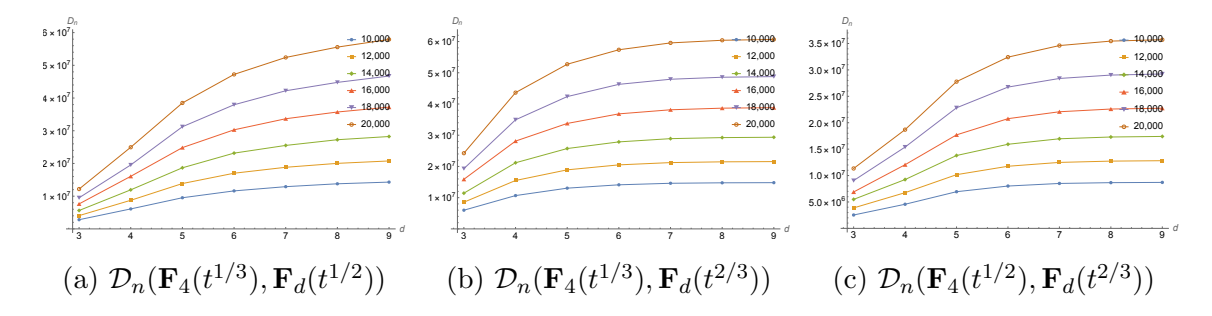


Figure 17: $\mathcal{D}_n(\mathbf{F}_4(p_1), \mathbf{F}_d(p_2))$ does not just depend on the difference in the dimension but also crucially on the different scale factors. Thus $\mathbf{F}_4(t^{1/3})$ is closer to $\mathbf{F}_3(t^{1/2})$ than to $\mathbf{F}_4(t^{1/2})$, and similarly, $\mathbf{F}_4(t^{1/3})$ is closer to both $\mathbf{F}_{2,3}(t^{2/3})$ than to $\mathbf{F}_4(t^{2/3})$.

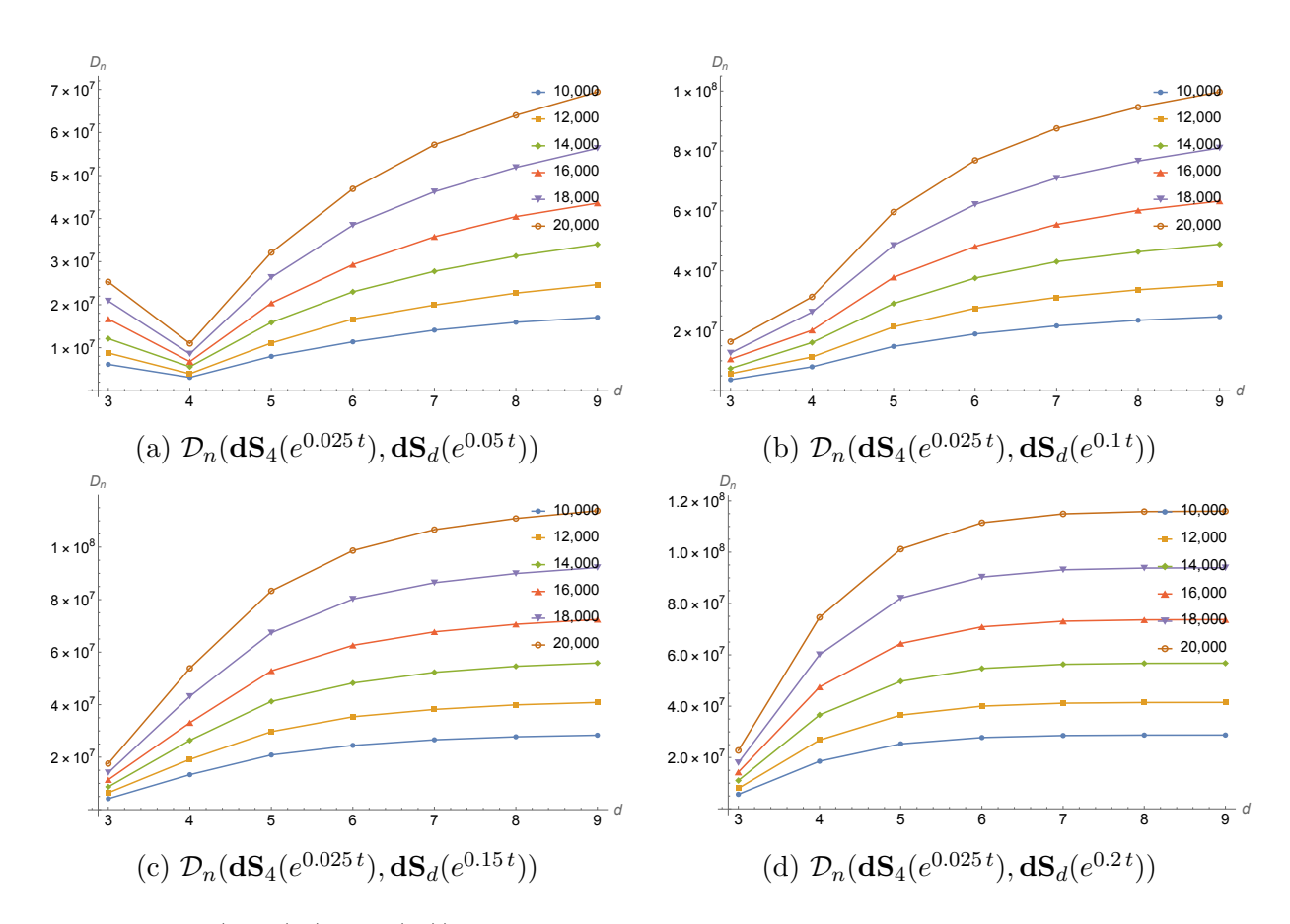


Figure 18: $\mathcal{D}_n(\mathbf{dS}_4(c_1), \mathbf{dS}_d(c_2))$ again does not just depend on the difference in the dimension but also on the different scale factors.

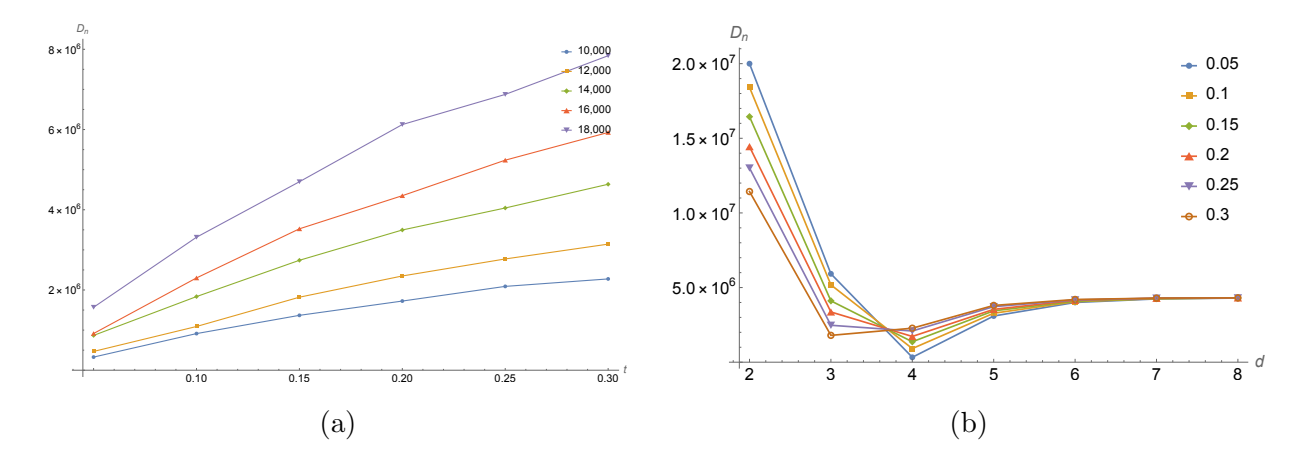


Figure 19: $\mathcal{D}_n(\mathbb{D}^4, \mathbb{D}^d \times \mathbb{I}_t)$ is shown as a function of d = 2, ... 8 and for various values of the thickness t. In (a) d = 4 and one varies over n and t, while in (b) n = 10,000 and one varies over d and t. Note that the minimum value $\mathcal{D}_n(\mathbb{D}^4, \mathbb{D}^4 \times \mathbb{I}_{0.05}) \sim 3 \times 10^5$ is not small!

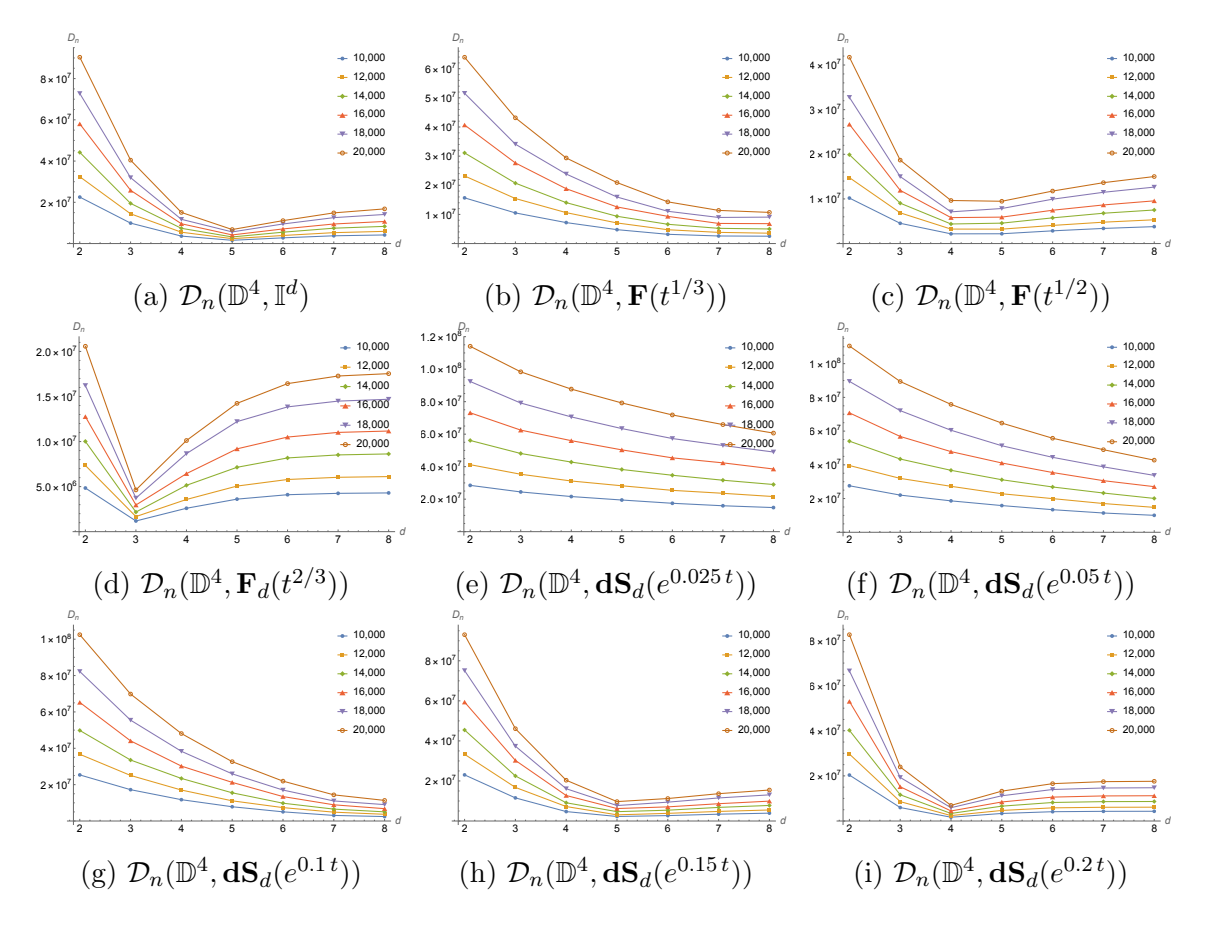


Figure 20: Plots of $\mathcal{D}_n(\mathbb{D}^4,.)$ for different spacetimes.

not a true distance function since it can vanish between non-isometric spacetimes. It is constructed from a family of order invariants $\mathbf{N}_m^{(n)}$ in the underlying n-element random causal sets associated with each spacetime. The $\mathbf{N}_m^{(n)}$ are the abundances of order intervals of size m whose expectation values define the n-interval spectrum $\mathcal{S}_n(M,g)$ of a spacetime (M,g) [36]. Using the map $\mathcal{S}_n(M,g) \to \mathbb{R}^{n-1}$, we define $\mathcal{D}_n^{(r)}(.,.)$ to be the L^r distance function on \mathbb{R}^{n-1} , which in turn provides a closeness function on \mathcal{L} . Without loss of generality we consider the r=1 case, i.e., the taxi-cab distance $\mathcal{D}_n(.,.) \equiv \mathcal{D}_n^{(1)}(.,.)$ on \mathbb{R}^{n-1} . We quotient \mathcal{L} by the equivalence class of interval isospectral spacetimes to define a notion of convergence on $\tilde{\mathcal{L}} = \mathcal{L}/\sim$. Because of interval isospectrality, $\mathcal{D}_n(.,.)$ is strictly weaker than Bombelli's closeness function but has the advantage that it can be numerically calculated for a wide range of spacetimes.

Despite the obvious drawback of interval isospectrality, our closeness function $\mathcal{D}_n(.,.)$ has its uses in Lorentzian geometry. In this work we have used it to define converge for monotonically increasing (or decreasing) scale factors in FRW-type spacetimes. When supplemented by a small set of additional order invariants, the convergence can be defined more generally. At present $\langle \mathbf{N}_m^{(n)}(M,g)\rangle$ has been calculated analytically for the d-dimensional Minkowski causal diamond \mathbb{D}^d . Extending this calculation to other spacetimes – for example, de Sitter or general Riemann Normal Neighbourhoods – would provide a better analytic understanding of the strengths and weaknesses of the current proposal.

The simulations in this work, though fairly extensive are largely for illustrative purposes. Constructing $\mathcal{D}_n(.,.)$ for a much wider trial set, as a catalogue of sorts, would expand the scope of the present work. There are of course other types of order invariant spectra like the abundance of m-element chains or the abundance of m-element past or future sets [40], from which closeness functions can be constructed on \mathcal{L} . Exploring these possibilities and comparing them with our closeness function would be a useful future direction to pursue.

In summary, our closeness function on $\tilde{\mathcal{L}}$ serves two purposes. The first is to quantify when an abstract causal set is continuumlike. The second is to define an approximate isometry between interval non-isospectral spacetimes, which in turn gives rise to a convergence condition on \mathcal{L} for certain sequences of spacetimes. The family of order invariants we have chosen in this work can be supplemented by other sets of order invariants, and in special cases yields stronger convergence conditions.

5 Acknowledgements

The author was supported in part by the ANRF MATRICS grant, MTR/2023/000831. She attended the 2nd Workshop on "A new geometry for Einstein's theory of relativity and beyond" at the University of Vienna thanks to the Austrian Science Fund (FWF) [Grant DOI 10.55776/EFP6]. She would like to thank the organisers of this meeting and the stimulating discussions that followed with the participants. She would also like to thank Dr. Emma Albertini for discussions.

References

- [1] L. Bombelli, J. Lee, D. Meyer, and R. Sorkin, "Space-Time as a Causal Set," *Phys. Rev. Lett.*, vol. 59, pp. 521–524, 1987.
- [2] J. A. Wheeler, "Superspace and the nature of Quantum Geometrodynamics," Adv. Ser. Astrophys. Cosmol., vol. 3, pp. 27–92, 1987.
- [3] A. E. Fischer, "The Theory of Superspace," in *Relativity Conference in the Midwest*, pp. 303–357, 1970.
- [4] D. A. Edwards, "The structure of superspace," in *Studies in Topology* (N. M. Stavrakas and K. R. Allen, eds.), pp. 121–133, Academic Press, 1975.
- [5] M. G. M., J. Lafontaine, and P. Pansu, Structures Metriques pour les varieties reimannienness. Paris: Cedric/Fernand Nathan, 1981.
- [6] P. Petersen, Riemannian Geometry. Springer, 2006.
- [7] J. K. Beem, P. Ehrlich, and K. Easley, Global Lorentzian Geometry. CRC Press, 3 1996.
- [8] L. Bombelli, "Statistical Lorentzian geometry and the closeness of Lorentzian manifolds," J. Math. Phys., vol. 41, pp. 6944–6958, 2000.
- [9] M. Braun, "Spacetime reconstruction by order and number," 7 2025.
- [10] J. Noldus, "A Lorentzian Lipschitz, Gromov-Hausdoff notion of distance," Class. Quant. Grav., vol. 21, pp. 839–850, 2004.
- [11] J. Noldus, "A new topology on the space of Lorentzian metrics on a fixed manifold," *Class. Quant. Grav.*, vol. 19, pp. 6075–6107, 2002.

- [12] L. Bombelli and J. Noldus, "The Moduli space of isometry classes of globally hyperbolic space-times," Class. Quant. Grav., vol. 21, pp. 4429–4454, 2004.
- [13] O. Müller, "Lorentzian gromov-hausdorff theory and finiteness results," 2022.
- [14] E. Minguzzi and S. Suhr, "Lorentzian metric spaces and their Gromov-Hausdorff convergence," *Lett. Math. Phys.*, vol. 114, no. 4, p. 90, 2024.
- [15] M. Kunzinger and R. Steinbauer, "Null Distance and Convergence of Lorentzian Length Spaces," *Annales Henri Poincare*, vol. 23, no. 12, pp. 4319–4342, 2022.
- [16] A. Mondino and C. Sämann, "Lorentzian Gromov-Hausdorff convergence and precompactness," 4 2025.
- [17] M. Braun and C. Sämann, "Gromov's reconstruction theorem and measured Gromov-Hausdorff convergence in Lorentzian geometry," 6 2025.
- [18] M. Kunzinger and C. Sämann, "Lorentzian length spaces," *Annals Global Anal. Geom.*, vol. 54, no. 3, pp. 399–447, 2018.
- [19] C. Sormani and C. Vega, "Null distance on a spacetime," Class. Quant. Grav., vol. 33, no. 8, p. 085001, 2016.
- [20] B. Allen and A. Burtscher, "Properties of the Null Distance and Spacetime Convergence," Int. Math. Res. Not., vol. 2022, no. 10, pp. 7729–7808, 2022.
- [21] A. Sakovich and C. Sormani, "The null distance encodes causality," *J. Math. Phys.*, vol. 64, no. 1, p. 012502, 2023.
- [22] A. Sakovich and C. Sormani, "Introducing Various Notions of Distances between Space-Times," 10 2024.
- [23] S. W. Hawking, A. R. King, and P. J. Mccarthy, "A New Topology for Curved Space-Time Which Incorporates the Causal, Differential, and Conformal Structures," J. Math. Phys., vol. 17, pp. 174–181, 1976.
- [24] D. B. Malament, "The class of continuous timelike curves determines the topology of spacetime," *Journal of Mathematical Physics*, vol. 18, no. 7, pp. 1399–1404, 1977.
- [25] E. H. Kronheimer and R. Penrose, "On the Structure of causal spaces," *Proc. Cambridge Phil. Soc.*, vol. 63, pp. 481–501, 1967.
- [26] S. Surya, "The causal set approach to quantum gravity," *Living Rev. Rel.*, vol. 22, no. 1, p. 5, 2019.

- [27] S. Surya, "The Causal Set Approach to Quantum Gravity," Lect. Notes Phys., vol. 1036, p. pp., 2025.
- [28] L. Bombelli and D. A. Meyer, "The Origin of Lorentzian Geometry," *Phys. Lett.*, vol. A141, pp. 226–228, 1989.
- [29] O. Müller, "On the hauptvermutung of causal set theory," 2025.
- [30] D. J. Kleitman and B. L. Rothschild, "Asymptotic enumeration of partial orders on a finite set," Transactions of the American Mathematical Society, vol. 205, pp. 205–220, 1975.
- [31] J. Myrheim, "Statistical geometry," Tech. Rep. CERN-TH-2538, CERN, 1978.
- [32] D. Meyer, The Dimension of Causal Sets. PhD thesis, M.I.T., 1988.
- [33] D. M. Benincasa and F. Dowker, "The scalar curvature of a causal set," *Phys.Rev.Lett.*, vol. 104, p. 181301, 2010.
- [34] F. Dowker and L. Glaser, "Causal set d'alembertians for various dimensions," *Classical and Quantum Gravity*, vol. 30, no. 19, p. 195016, 2013.
- [35] L. Glaser, "A closed form expression for the causal set d'alembertian," Classical and Quantum Gravity, vol. 31, no. 9, p. 095007, 2014.
- [36] L. Glaser and S. Surya, "Towards a Definition of Locality in a Manifoldlike Causal Set," Phys. Rev., vol. D88, no. 12, p. 124026, 2013.
- [37] S. Surya, "Evidence for the continuum in 2d causal set quantum gravity," Classical and Quantum Gravity, vol. 29, p. 132001, July 2012.
- [38] L. Glaser and S. Surya, "The Hartle–Hawking wave function in 2D causal set quantum gravity," Class. Quant. Grav., vol. 33, no. 6, p. 065003, 2016.
- [39] W. J. Cunningham and S. Surya, "Dimensionally Restricted Causal Set Quantum Gravity: Examples in Two and Three Dimensions," Class. Quant. Grav., vol. 37, no. 5, p. 054002, 2020.
- [40] R. Sorkin and N. Zwane, Unpublished.